International Journal of GEOMATE, March., 2021, Vol.20, Issue 79, pp. 68-73
ISSN: 2186-2982 (P), 2186-2990 (O), Japan, DOI: https://doi.org/10.21660/2021.79.GX189
Geotechnique, Construction Materials and Environment

ANALYSIS OF EMBANKMENT STRESS PRODUCED DURING CONSTRUCTION AND IN-SERVICE PHASES CONSIDERING EMBANKMENT GEOMETRIES

*Shin-ichi Kanazawa[1] and Haruna Igarashi[2]

[1]National Institute of Technology, Fukushima College, Japan; [2]OYO Co., Ltd, Japan

*Corresponding Author, Received: 21 Jul. 2020, Revised: 07 Jan. 2020, Accepted: 28 Jan. 2021

ABSTRACT: Soil compaction tests are carried out to improve embankment construction engineering characteristics, such as stability and deformation. For construction, enclosed embankment structures perform total strengthening and a measure of drainage functions. This provides stability, improves deformation properties, and prevents the degradation or rot of objects placed in the embankment fill. Nevertheless, chances are that inadequate compaction will cause material, such as rocks or stones, to fall from the slope surface, as well as erosion. Therefore, the standards for embankment slope steepness set forth the use of a 1:1.8 ratio, permissible on an as-needed basis to allow for mechanical rolling for compaction. When constructing steep embankment slopes, it is necessary to conduct embankment stability checks and fully consider the provision of slope protection to prevent erosion. However, differences in stress conditions attributable to varying slope steepness have not been elucidated. In this study analyzes embankment construction in terms of different construction seasons and slope change, using the unsaturated soil-water-air coupled FEM analysis program. In this way, more accurate qualitative evaluation could be achieved.

Keywords: Embankment Geometries, Unsaturated soil, Compaction, Finite element analysis

1. INTRODUCTION

In recent years, torrential rain and other extreme weather events have caused frequent disasters across the world. It is urgently necessary to establish an analysis technique to continuously evaluate and examine the quality of embankment structures during construction and in-service phases. In this regard, it is important to determine the initial stress. Normally, embankment structures are made up of compacted earth in order to improve stability and deformation properties. However, existing reports present many cases of collapsed embankment structures that fail due to torrential rains.

Currently, to evaluate embankment stability against heavy rains, Embankment relies heavily on four factors: treatment of foundation ground, quality of embankment materials, degree of compaction, and handling of water. Specifically, the guidelines place importance on drainage [1]. In addition, engineers rely on rules of thumb in carrying out embankment work, maintenance, and management. Considering these conditions, it is highly probable that, in the future, importance will be placed on embankment maintenance and management against torrential rains.

Another set of important factors includes embankment drainage measures and when the embankment is subjected to the effects of rainfall. Drainage measures taken against rainfall during embankment construction differ from those taken during the in-service phase. Rainfall affects the embankment intermittently after the commencement of construction and during the in-service phase. Accordingly, rainfall during construction may change stress conditions inside the embankment. However, embankments are constructed in no specific season and are subject to various levels of rainfall during construction. Generally, embankments are not constructed in the rainy season; although, occasionally, this happens for unavoidable reasons. In such cases, attention is paid to weather, and drainage measures are implemented. Moreover, embankments are subject to climate conditions, such as repeated drying and wetting cycles. Therefore, the effects of stress behavior occurring during transitions between unsaturated and saturated conditions are not negligible. Hence, to estimate the initial stress conditions taking place after embankment construction, it is important to consider the effects of dry and wet climate conditions [2]. This leads to the need for analysis techniques that consider climatic conditions, such as rainfall and evaporation [3][4]. Moreover, differences in the steepness of embankment slopes are an important factor. Standards are in place that specify embankment slope steepness for different embankment materials and heights. In general, low embankments are regarded as not at risk for a major collapse if their slope steepness is 1:1.5 and their construction is

sound. This does not apply to those embankment materials that are problematic, specifically in terms of quality. However, at the slope steepness of 1:1.5, the slope face is unlikely to receive adequate compaction. Chances are that inadequate compaction will cause material, such as rocks or stones, to fall from the slope surface, as well as erosion. Therefore, the standards for embankment slope steepness set forth the use of a 1:1.8 ratio, permissible on an as-needed basis to allow for mechanical rolling for compaction. When constructing steep embankment slopes, it is necessary to conduct embankment stability checks and fully consider the provision of slope protection to prevent erosion. However, differences in stress conditions attributable to varying slope steepness have not been elucidated.

To meet this challenge, this study analyzes embankment construction in terms of different construction seasons and slope change, using the unsaturated soil-water-air coupled FEM analysis program (DACSAR-MP) [5].

2. RESEARCH METHOD

2.1 Soil/Water/Air Coupled Finite Analysis Code

The finite element analysis code used in this study formulates the unsaturated soil constitutive model proposed by Ohno et al [6]. This model is framed as the soil/water/air coupled problem using the three-phase mixture theory. Equation (1) shows the effective stress. Equation (2) shows the base stress tensor and suction stress. Equation (3) shows suction.

$$\boldsymbol{\sigma}' = \boldsymbol{\sigma}^{\mathbf{net}} + p_s \mathbf{1} \tag{1}$$

$$\boldsymbol{\sigma}^{\mathbf{net}} = \boldsymbol{\sigma} - p_a \mathbf{1},\ p_s = S_e s \tag{2}$$

$$s = p_a - p_w, S_e = \frac{S_r - S_{rc}}{1 - S_{rc}} \tag{3}$$

Here, $\boldsymbol{\sigma}'$ is the effective stress tensor; $\boldsymbol{\sigma}^{\mathbf{net}}$ is the base stress tensor; $\mathbf{1}$ is the second order unit tensor; $\boldsymbol{\sigma}$ is the total stress tensor; s is the suction; p_s is the suction stress; p_a is the pore air pressure; p_w is the pore water pressure; S_r is the degree of saturation; S_e is the effective degree of saturation; and S_{rc} is the degree of saturation at s→∞. Equations (4), (5), (6) and (7) provide the yield function.

$$f\left(\boldsymbol{\sigma}', \zeta, \varepsilon_v^p\right) = MD \ln \frac{p'}{\zeta p_{sat}'} + \frac{MD}{n_E}\left(\frac{q}{Mp'}\right)^{n_E} - \varepsilon_v^p = 0 \tag{4}$$

$$\zeta = \exp\left[\left(1 - S_e\right)^{n_s} \ln a\right], MD = \frac{\lambda - \kappa}{1 + e_0} \tag{5}$$

$$p' = \frac{1}{3}\boldsymbol{\sigma}' : \mathbf{1}, q = \sqrt{\frac{3}{2}\mathbf{s} : \mathbf{s}} \tag{6}$$

$$\mathbf{s} = \boldsymbol{\sigma}' - p'\mathbf{1} = \mathbf{A} : \boldsymbol{\sigma}', \mathbf{A} = \mathbf{I} - \frac{1}{3}\mathbf{1} \otimes \mathbf{1} \tag{7}$$

Here, n_E is the shape parameter; ε_v^p is the plastic volume strain; M is the *q/p'* in the limit state; D is the dilatancy coefficient; p_{sat}' is the yield stress at saturation; a and n_s are the parameters representing the increase in yield stress due to unsaturation; λ is the compression index; and κ is the expansion index. Equation (8) shows pore water velocity. Equation (9) shows air velocity. Porewater and air flow follow Darcy's law.

$$\tilde{v}_{\mathrm{w}} = -\mathbf{k}_{\mathbf{w}} \cdot \mathrm{grad} h \tag{8}$$

$$\tilde{v}_{\mathrm{a}} = -\mathbf{k}_{\mathbf{a}} \cdot \mathrm{grad} h_a, h_a = \frac{p_a}{\gamma_w} \tag{9}$$

Here, $\tilde{v}_{\mathrm{w}}$ is the pore water velocity; $\tilde{v}_{\mathrm{a}}$ is the air velocity; $\mathbf{k}_{\mathbf{w}}$ is the hydraulic conductivity; $\mathbf{k}_{\mathbf{a}}$ is the coefficient of air permeability; h is the total head; γ_w is the unit weight of water; and h_a is the pneumatic head. Equations (10)-(11) show hydraulic conductivity and the coefficient of air permeability by way of Mualem's [7] formula and the Van Genuchten [8] formula.

$$\mathbf{k}_{\mathbf{w}} = k_{rw}\mathbf{k}_{\mathbf{wsat}} = S_e^{1/2}\left[1 - \left(1 - S_e^{1/m}\right)^m\right]^2 \mathbf{k}_{\mathbf{wsat}} \tag{10}$$

$$\mathbf{k}_{\mathbf{a}} = k_{ra}\mathbf{k}_{\mathbf{ares}} = \left(1 - S_e\right)^{1/2}\left(1 - S_e^{1/m}\right)^{2m} \mathbf{k}_{\mathbf{ares}} \tag{11}$$

Here, k_{rw} is the ratio of hydraulic conductivity; k_{ra} is the ratio of coefficient of air permeability; m is the Mualem constant; $\mathbf{k}_{\mathbf{wsat}}$ is the hydraulic conductivity at saturation; $\mathbf{k}_{\mathbf{ares}}$ is the coefficient of air permeability in dry conditions. Equations (12)-(13) show the continuous formula of pore water and air using three-phase mixture theory.

$$n\dot{S}_r - S_r\dot{\varepsilon}_v + \mathrm{div}\tilde{v}_w = 0 \tag{12}$$

$$\left(1 - S_r\right)\dot{\varepsilon}_v + n\dot{S}_r - n\left(1 - S_r\right)\frac{\dot{p}_a}{p_a + p_0} - \mathrm{div}\tilde{v}_a = 0 \tag{13}$$

Here, n is porosity; $\dot{\varepsilon}_v$ is volumetric strain; and p_0 is atmospheric pressure. The elasto-plastic constitutive model obtained from Equation (4) and the equilibrium equation [Equations (12) - (13)] are formulated as the soil/water/air coupled problem.

3. ANALYSIS CONDITIONS

3.1 Analysis Conditions

Table 1 and Fig. 1 show analysis material parameters used for both foundation ground and embankment and moisture characteristic curves [9] [10]. The value was obtained by experiment. Figure 3 shows the embankment used for analysis and its analysis regions. Regarding the size of the analysis region, the foundation ground was set to 15 m long and 45 m wide and the embankment was set to 3 m and 15 m long at the top and bottom, respectively, and 6 m high. The foundation ground was set as saturated between the ground level and 3 m above ground level. Slopes were set to three levels: 1:1, 1:1.5, and 1:2. The construction period was set to one month. After being laid down, each individual 30 cm layer was subjected to loading and unloading pressures of 500 kPa to represent compaction. For displacement boundaries, the lower end of the foundation ground was fixed in the vertical and horizontal directions. These conditions were used to conduct a plane strain analysis (Ignore depth). The water level boundaries of the foundation ground were set to be drained at the top and bottom boundaries and undrained at the right and left boundaries. Regarding drainage measures, a drainage layer (3 m long and 0.6 m high) was provided at the toe of the slope, and the entire slope face was covered with vegetation mats as a root element (to consider only evaporation effects). The water permeability coefficient of the drainage layer was set to 500 times that of the embankment, with the air permeability coefficient being 100 times the water permeability coefficient. Other conditions specified in the Embankment Earthwork Guidelines were also fulfilled. Figure 2 shows rainfall conditions [11] used for the analysis. Amounts of rainfall observed in 2016 in Utsunomiya, Tochigi Prefecture were used as rainfall conditions to simulate the average amount of rainfall in Japan (approx.1,750mm/year). The analysis selected spring, summer, fall, and winter seasons, as shown in the figure. For the analysis, the embankment construction process was assigned a seasonally averaged daily amount of rainfall. Evaporation rates were also matched with rainfall seasons.

Subsequent to an analysis of initial stresses inside embankment, observations of differences with embankment construction season1, and an analysis of stresses in embankments in service for 10 years, this study evaluated embankment failure, assigning embankment treatments of 10 mm to 50 mm per hour rainfall. These were applied as torrential rainfall for 1h and continuous rainfall for 5h.

Table 1 Material Parameter

λ	κ	M	m	S_{r0}	k_a
0.18	0.037	1.33	0.8	0.15	1.00
n	n_E	a	v	G_s	k_w
1.0	1.3	10.0	0.33	2.7	0.01

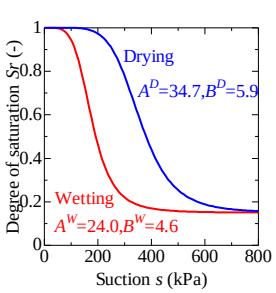

Fig.1 Moisture characteristic curve

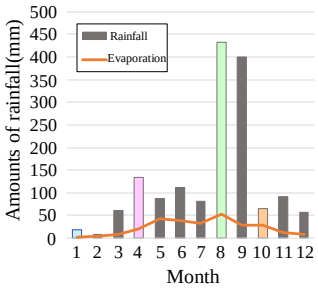

Fig.2 Rainfall condition

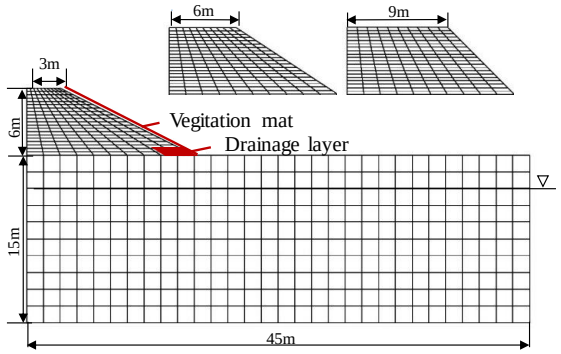

Fig. 3 Analysis mesh

3.4 Stress Change inside Embankments in Service for 10 Years, Noting Contributions of Differences in Slope Face

Figure 4 summarizes analysis results for embankments in service for 10 years in terms of mean effective stress, void ratio, deviatoric stress, suction, shear strain, and critical state determination ratio.

First, the foundation ground will be examined. The values of mean effective stress are high with respect to all angles (I). The values represented in the void ratio distributions are small for all seasons (II). These results are interpreted as fully demonstrating compaction effects according to the relationships between void ratio and effective stress.

Next, the mean effective stress values inside embankment will be compared, noting seasonal differences. According to I, values are high in winter when the amount of rainfall is small. In contrast, values are low in summer when the amount of rainfall is large. Meanwhile, according to II, the void ratio values are lower in winter than in summer. In summer, values are high in the slope area. Probable causes of these results are volumetric expansion due to rainfall and the loss of suction in

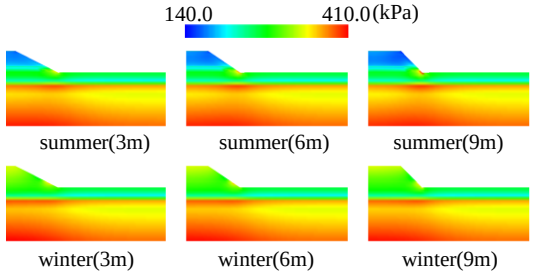

(I) Mean effective stress

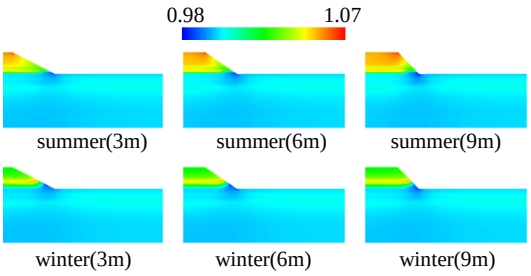

(II) Void ratio

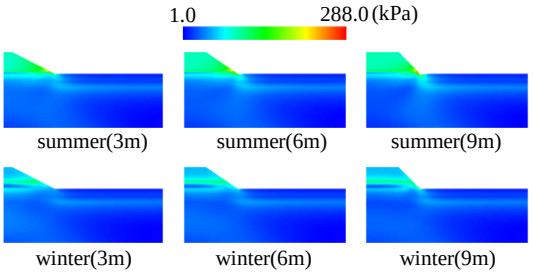

(III) Deviator stress

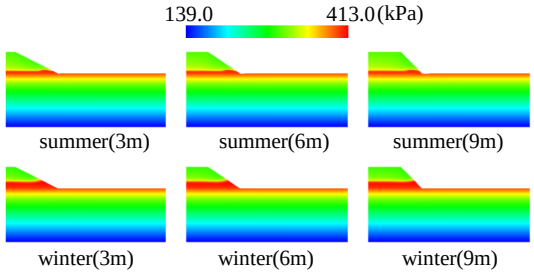

(IV) Suction

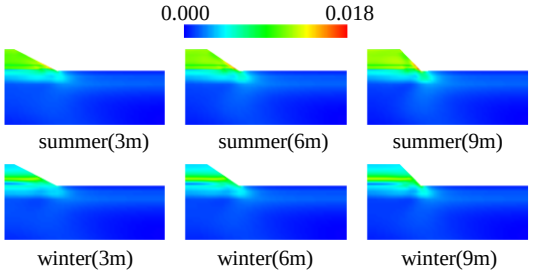

(V) Shear strain

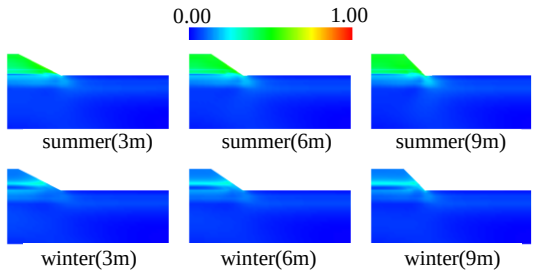

(VI) Critical state determination ratios

Fig. 4 Summarizes analysis results

summer, as represented by the suction distribution (IV). Moreover, strength and deformation properties improve with increasing suction (decreasing degree of saturation). Consequently, the internal strength of the embankment is likely to be high in the low rainfall seasons. Shear strain values are low in winter as revealed by shear strain distributions (V), while in summer, a slight sign of rotational slip is present. The maximum shear strain value is approximately 1.8%, at which a failure can occur if torrential rain or other extreme weather conditions occur.

A comparison considering angle differences reveals that according to I, mean effective stress values at the toe of the slope are larger for cases of embankment having a 9 m long top than with embankment having a 3 m long top. Additionally, according to II, void ratio values at the toe of the slope are small. This is interpreted to mean that at higher slope angles, compressive forces are applied more intensively to the toe of the slope. Meanwhile, shear strain values (V) at the toe of the slope are higher for embankment with a 9 m long top than for embankment with a 3 m long top. The critical state determination ratios (VI) indicate no risk of failure under the current conditions. However, at steeper slope angles, the risk of failure is likely high, notably at the toe of the slope.

Figure 5 presents matrices showing results that represent the relationship between the amount and duration of rainfall (in Summer). The analysis assumed that risk of failure was present at levels of 3% or higher shear strain and 1.00 or higher critical state determination ratios. Cases with no concern about failure are indicated with a circle (Blue) and those with a concern about failure are indicated with a cross (Yellow). Generally, concern about failure was present with increasing amount and duration of rainfall. The matrices reveal no difference between varying slope steepness.

To understand rainwater infiltration conditions at average rainfall intensity, Fig. 6 shows stress distributions rendered thorough an analysis of continued rainfall at 30 mm/h. Top contour diagrams represent stress conditions inside the embankment immediately following 5 h of 30 mm/h rainfall. Bottom graphs show the relationships between the analysis period and individual stresses, revealing changes over time in each stress. The colors of the curves correspond to the colors of embankment elements shown in the middle.

3m		Rainfall duration				
		1 hour	2 hours	3 hours	4 hours	5 hours
Rainfall	10mm					
	20mm					
	30mm					
	40mm					
	50mm					

6m		Rainfall duration				
		1 hour	2 hours	3 hours	4 hours	5 hours
Rainfall	10mm					
	20mm					
	30mm					
	40mm					
	50mm					

9m		Rainfall duration				
		1 hour	2 hours	3 hours	4 hours	5 hours
Rainfall	10mm					
	20mm					
	30mm					
	40mm					
	50mm					

Fig. 5 Matrices showing results

The mean effective stress values (I) are low at the top and slope face, which were areas with assigned rainfall. The values at the toe of the slope increase with increasing slope steepness. The graphs also reveal that the mean effective stress values at the toe of the slope are higher with increasing steepness of embankment, and that as rainfall continues, values inside the embankment increase while values at the slope face decrease.

The degree of saturation values (II) at the toe of the slope are low. Therefore, the drainage layer is satisfactorily functional. The values are high at the top and slope face, which were assigned rainfall, with no sign of rainwater infiltration into the embankment interior. This ascertains that moisture infiltrates the embankment along the surface layer. This is interpreted to mean that because of the rapid rate of rainfall assigned, the moisture had little time to enter the inner part of the embankment and thus flowed through the surface layer. Specifically, the analysis techniques used in this study accounted for ground infiltration capacity. The computation took ground infiltration capacity into account so as not to allow rainfall to cause a positive pore pressure at the ground level. Therefore, the surface layer water flow was rendered, and this simulation suggested, as a result, the formation of a surface layer slip. Moreover, the degree-of-saturation values inside the embankment and at the toe of the slope are virtually constant against the passage of time, as shown by the graphs. The values at the toe of slope are high due to rainfall after embankment construction.

Void ratio values (III) at the toe of the slope are low, with smaller values occurring more intensively

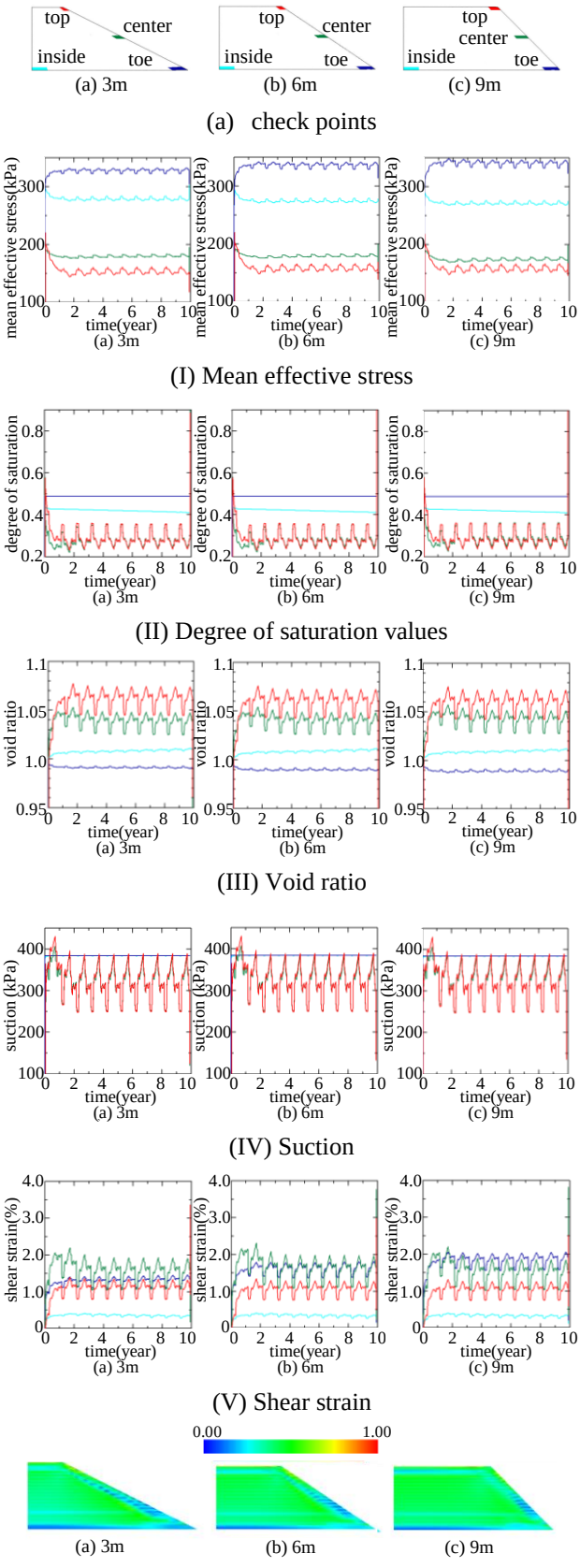

Fig. 6 Summarizes analysis results

at the toe of the slope with increasing slope steepness. The graphs also reveal that the void ratio values are higher, although slightly, at the center of the slope face, while the values are of lower intensity at the toe of the slope with increasing slope steepness. The values decrease substantially along the slope face due to rainfall.

Suction values (IV) are low at the top and slope face of the embankment, which are areas assigned rainfall. Because strength and deformation properties increase with increasing suction, it is highly probable that the strength of the slope is low. Moreover, the graphs reveal virtually constant suction values inside the embankment and at the toe of the slope where the drainage layer is present. Suction values at the slope face are largely affected by the amount of rainfall and substantially decrease due to rainfall.

Shear strain values (V) are high at the top and slope face of the embankment, which are areas assigned rainfall. The values at the toe of the slope are higher with increasing slope steepness. The graphs also show that shear strain values at the slope face increase due to rainfall and that the values at the toe of slope are higher with increasing slope steepness. This suggests the presence of vulnerable regions at the top and along the slope face, the emergence of vulnerable regions at the toe of the slope with increasing slope steepness, and resultant higher risks of embankment failure.

The critical state determination ratios (VI) prove no risk of failure under the current conditions. Nonetheless, at higher slope steepness, failure risks are thought to be high at the toe of the slope.

These findings indicate the occurrence of vulnerable regions at the top and along the slope, the emergence of vulnerable regions at the toe of the slope with increasing slope steepness, and higher risks of embankment failure as a result of torrential rains on an embankment in service for 10 years. Meanwhile, neither shear strain nor critical state determination ratios exceeded the set limits.

4. CONCLUSION

Using the unsaturated soil-water-air coupled FEM analysis program (dissolved-air model), this study provided an analytical representation of stress changes in embankment caused by rainfall during construction and internal mechanical behaviors of embankment assigned torrential rains during the in-service phase.

Although matrices and contour diagrams showed little differences in stress conditions between varying slope steepness, graphs drawn to describe changes in individual stress conditions against the passage of time made differences in stress conditions visually clear between varying levels of slope steepness.

Future challenges include simulating the embankment construction phase using the properties of soil materials from actual ground. In this way, more accurate qualitative evaluation could be achieved. It is necessary to conduct analyses simulating actual torrential rains in the future, using analysis conditions better representing the natural environment.

5. REFERENCES

[1] Japan Road Association,: Roadway Workers - Fill Construction Guidelines, 2010.

[2] Nishi K., Fukukawa K., Ogawa T., and Nakagawa K.: A System for forecasting cut-off slope collapse during continuous heavy rain, Journal of JSCE, Vol.24, No.498, pp.95-104, 1994.

[3] Kanazawa S., Tachibana S., Iizuka A.: Analytical study on drainage capacity of embankment structure, Journal of JSCE, Vol.71, pp.429-436, 2015.

[4] Kanazawa S, Suzuki S: Stress analysis of embankment due to different in construction conditions, International Journal of GEOMATE , 18(65), 2020.

[5] Kanazawa S., Toyoshima K., Kawai K., Tachibana S. and Iizuka A.: Analysis of mechanical behavior of compacted soil with F.E. method, journal of JSCE, No.68 (2), pp.291-298, 2012.

[6] Ohno S., Kawai K., and Tachibana S.: Elasto-plastic constitutive model for unsaturated soil applied effective degree of saturation as a parameter expressing stiffness, Journal of JSCE, Vol.63/No.4, pp.1132-1141,2007.

[7] Mualem Y.: A new model for predicting the hydraulic conductivity of unsaturated porous media, Water Re-sources Research, Vol.12, No.3, pp.514-522, 1976.

[8] Van Genuchten: A closed-form equation for predicting hydraulic of unsaturated soils, Soil Science Society American Journal, Vol.44, pp.892-898, 1980.

[9] Kawai K., Wang W. and Iizuka A.: The expression of hysteresis appearing on water characteristic curves and the change of stresses in unsaturated soils, Journal of applied mechanics, Vol.5, pp.777-784,2002.

[10] Sugii T. and Uno T.: Modeling the New Moisture Characteristic Curve, Journal of JSCE, pp.130-131, 1995.

[11] Japan Meteorological Agency : http://www.jma.go.jp/jma/index.html.